International Journal of Biological Macromolecules 212 (2022) 193–201

Contents lists available at ScienceDirect

International Journal of Biological Macromolecules

journal homepage: www.elsevier.com/locate/ijbiomac

Structural characterization of a homopolysaccharide produced by *Weissella cibaria* FMy 2-21-1 and its potential application as a green corrosion inhibiting film

René Emanuel Lobo [a], Patricio Andrés Orrillo [b], Susana Beatriz Ribotta [b], Graciela Font de Valdez [a], Mercedes Santos García [c], José Carlos Rodríguez Cabello [c], María Inés Torino [a,*]

[a] Centro de Referencia para Lactobacilos (CERELA)–CCT CONICET NOA Sur, Batalla de Chacabuco 145, San Miguel de Tucumán 4000, Tucumán, Argentina
[b] Instituto de Química del Noroeste Argentino (INQUINOA) – Universidad Nacional de Tucumán (UNT) – CCT CONICET NOA Sur, Instituto de Química Física, Facultad de Bioquímica, Química y Farmacia, UNT, Batalla de Ayacucho 471, San Miguel de Tucumán 4000, Tucumán, Argentina
[c] BIOFORGE (Group for Advanced Materials and Nanobiotechnology), University of Valladolid, CIBER-BBN, 47011 Valladolid, Spain

ARTICLE INFO

Keywords:
HoPS structure
Biocoating
Corrosion inhibitor

ABSTRACT

Steel corrosion is a global issue that affects safety and the economy. Currently, the homopolysaccharide (HoPS) structure of a novel lactic acid bacterium (LAB) is under study, as well as its application as a green corrosion inhibitor. *Weissella cibaria* FMy 2-21-1 is a LAB strain capable of producing HoPS in sucrose enriched media. The isolated and purified HoPS was characterized by different spectroscopic analyses as a linear α-1,6 dextran adopting a random coil conformation, with high molecular weight and extended size in water. The polysaccharide showed a semi-crystalline organization, which is a requirement for film formation. Its biocoating showed a grainy network structure, with a slightly lesser hydrophobic role in the aqueous environment than in the ionic one. The electrochemical measurements of the steel-HoPS coating showed that the biopolymer layer acts as an anodic-type corrosion inhibitor, with high resistance to corrosion by water and with chloride ions which prevent pitting, a corrosion process typical of bare steel. Few reports have cited the application of LAB HoPS as corrosive coating inhibitors. This work is the first to explore the influence of a structurally characterized dextran from *Weissella cibaria* strain as a potential steel corrosion inhibitor in ionic environments.

1. Introduction

Steel is one of the structural materials most widely used in industry on account of its low cost, endurance, malleability, ductility, and other mechanical properties. However, the high reactivity and thermodynamic instability of mild steel make it susceptible to corrosion [1,2], which causes damage, renders the material unattractive, and eventually leads to environmental pollution. Every country spends about 3.5% of its gross domestic product to solve problems caused by corrosion [2,3]. Even though various methods are available for corrosion control, organic heterocyclic compounds are time-tested inhibitors, highly recommended for industrial uses. They contain electron-rich heteroatoms (such as nitrogen, sulfur, and oxygen) that quickly form a metal-coordinated bond and form a layer. This physical barrier prevents further metal dissolution [2,4,5]. Waterborne polymer dispersions or latexes are widely used as primers for metal substrates. However, latexes are usually combined with expensive anticorrosive pigments, such as zinc phosphate, a procedure that is not sustainable and that has become one of the central topics of discussion in the coating industry [6]. Other synthetic organic inhibitors have also been reported as toxic for humans and the environment, either during their preparation or in their application [4,7].

Biopolymers (polysaccharides, proteins, lipids, and nucleic acids) are promising green corrosion inhibitors [8]. They are giant molecules containing more heteroatoms, which accelerate adsorption on metal surface and control corrosion. In addition, they are readily available, non-toxic, and biodegradable [2,4].

Previous research has shown that exopolysaccharides produced by

* Corresponding author at: Centro de Referencia para Lactobacilos (CERELA), Batalla de Chacabuco 145, San Miguel de Tucumán 4000, Tucumán, Argentina.
E-mail addresses: elobo@cerela.org.ar (R.E. Lobo), patricio.orrillo@fbqf.unt.edu.ar (P.A. Orrillo), susana.ribotta@fbqf.unt.edu.ar (S.B. Ribotta), gfont@cerela.org.ar (G.F. de Valdez), msantos@bioforge.uva.es (M.S. García), roca@bioforge.uva.es (J.C.R. Cabello), mitorino@cerela.org.ar (M.I. Torino).

https://doi.org/10.1016/j.ijbiomac.2022.05.105
Received 9 September 2021; Received in revised form 9 May 2022; Accepted 14 May 2022
Available online 18 May 2022

microorganisms have anticorrosive properties. Particularly, studies on the potential of homopolysaccharides (HoPS) to protect steel have led to exciting findings [6]. In addition, microbial biopolymers usually exhibit more productivity and are less resource-intensive than other natural sources (plants, algae, and animals). In this sense, the yield of the process could be enhanced by optimizing the operating conditions (e.g., pH, temperature, and agitation), developing high yield strains (e.g., genetic manipulation), or using cheap substrates [9]. In this context, lactic acid bacteria (LAB) have become industrially relevant microorganisms worldwide due to their qualified presumption of safety (QPS) status, and their use in the food industry, and in the biotechnology and therapeutics fields [10]. Certain LAB strains can produce an extracellular HoPS α-D-glucan type (polysaccharides formed by glucose units) in sucrose enriched media. Usually, these polymers are synthesized in large amounts (>1 $g{\cdot}L^{-1}$) by an extracellular free or cell-anchored glucansucrase, which uses sucrose glycosidic bond energy to extend the polymerization of glucosyl units [11]. Based on the glycosidic linkages present in the main chain, α-D-glucans are classified into (i) dextrans: α-(1, 6) with some α-(1, 2), α-(1, 3), or α-(1, 4) branches; (ii) mutans: α-(1, 3) with an α-(1, 6) branch; (iii) alternans: with alternating α-(1, 6) and α-(1, 3) linkages; and (iv) reuterans: α-(1, 4) with some α-(1, 6) branches. The structural features of the HoPS (branch linkage-type, molecular mass, or chain conformation) support their industrial application in biomaterial design, medicine, and food processing, among other areas [3,11]. Some LAB HoPS, such as α-(1, 3; 1, 6)-D-glucan from *Limosilactobacillus reuteri* 180, α-(1, 4)-D-glucan with an α-(1, 6) branch from *Limosilactobacillus reuteri* SK24.003a, and the dextran produced by *Leuconostoc mesenteroides* NRRL B-1498 have been reported as corrosion inhibiting coatings [3,12,13]. By replacing synthetic resins with polysaccharides, it is possible to decrease the emission of volatile organic compounds by coating factories, and their dependence on petroleum products, an important goal in modern societies [14].

Bioprospecting and characterizing new, natural, eco-friendly, safe, low-cost, and sustainable anticorrosive films is key to dealing with corrosion, a global issue that affects the appearance and performance of metal surfaces, with a high industrial, economic, and even environmental impact. Hence, the present study aimed to characterize the structure of a HoPS produced by *Weissella* (*W.*) *cibaria* FMy 2-21-1 in sucrose enriched media, by carefully considering its backbone structure, molar mass, and molecular conformation. Furthermore, the potential of this HoPS as an eco-friendly corrosion inhibitor film was also assessed through an analysis of its surface structure and electrochemical behavior on steel support in an ionic environment.

2. Materials and methods

2.1. HoPS production and isolation

W. cibaria FMy 2-21-1 was kindly provided by Dr. F. Mozzi (CERELA-CONICET CCT NOA Sur, Argentina). The strain was made to produce HoPS under 30 °C for 48 h in De Man, Rogosa, and Sharpe (MRS) agar, supplemented with 40 $g.L^{-1}$ sucrose (MRS + S), instead of glucose. The mucoid substance was recovered directly from the surfaces of the plates and processed as described by Lobo, Figueroa, Navarro, Gómez, de Valdez, and Torino [11]. Briefly afterwards, the HoPS was collected directly from the plates with a physiological solution, and was immediately centrifuged (9000 ×*g* for 10 min at 4 °C; Sorvall BP-8, Thermo Scientific, Massachusetts, USA) to discard bacterial cells. The cell-free supernatant was deproteinized with trichloracetic acid (12%, $w{\cdot}v^{-1}$), incubated at 4 °C for 2 h, and centrifuged (9500 ×*g*, 12 min, 4 °C). Subsequently, the polymer substance was precipitated from the supernatant by adding three volumes of cold ethanol (96%) and incubating at −20 °C for 48 h. Precipitated HoPS was recovered by centrifugation (20,000 ×*g*, 30 min, 4 °C), with subsequent dissolution in 5 mL deionized water for a second deproteinization phase, and other precipitation sessions followed in order to eliminate the remaining proteins. Next, the HoPS substance was dissolved in deionized water, dialyzed (MWCO 10000, Thermo Scientific Inc., Massachusetts, USA) against deionized water at 4 °C for 48 h, and lyophilized (LyoAlfa 10, Azbil Telstar, S.L., Barcelona, Spain). Finally, the mass of the polymer was measured (g HoPS·kg $medium^{-1}$) with an analytical scale, and it was stored at 4 °C for further analysis.

2.2. Purity analysis

The HoPS purity was determined according to the procedure described by Lobo, Gómez, de Valdez and Torino [15]. Briefly, a HoPS solution was prepared with deionized water (5 $mg{\cdot}mL^{-1}$), stored overnight at −20 °C, thawed quickly, and centrifuged (20,000 ×*g*, 20 min, 4 °C) to examine the precipitate formation. Then, protein content was analyzed using a kit assay according to the manufacturer's instructions (Bio-Rad Laboratories Inc., USA). Furthermore, ultraviolet (UV)-visible spectrum was recorded using a UV microplate reader (Biotek, Vermont, USA) between 200 and 550 nm to determine the presence of contaminants (proteins, nucleic acids, and pigments).

2.3. Fourier-transformed Raman (FT-R) and surface-enhanced Raman scattering (SERS)

The FT-R and SERS spectra of the HoPS were obtained in solid and colloidal silver nanoparticles (AgNPs), respectively, by using a DXR Raman microscope instrument (Thermo Fisher Scientific, Waltham, Massachusets, USA) with charge coupled device detector. The laser lines used were 532 nm (FT-R) and 780 nm (SERS). The spectral resolution was 4 cm^{-1} in the range 3500–50 cm^{-1}. The output laser powers were 10 mW (FT-R) and 24 mW (SERS); a confocal aperture of 50 mm slit with 100 (FT-R), and 40 (SERS) expositions of 4 s were accumulated to achieve an adequate signal-to-noise ratio. Also, SERS samples were carried out with the biopolymer in AgNPs solution (20 $mg.mL^{-1}$) kept at 4 °C for 12 h. The AgNPs were synthesized following the protocol of Lee and Meisel [16] with some modifications. 200 mL solution containing silver nitrate (5.10^{-4} M) and sodium citrate (3.10^{-3} M) was prepared. Subsequently, 4 mL of sodium borohydride (3.10^{-3} M) was added dropwise for the silver reduction. Finally, AgNPs were subsequently characterized by scanning electron microscopy (SEM), energy-dispersive X-ray spectrometry (EDS), and UV spectroscopy (Synergy HT, Biotek Instrument, Vermont, USA). SEM and EDS belong to facilities of CIME–UNT–CONICET CCT NOA Sur, Argentina. Commercial dextran (2000 kDa, Merck KGaA, Darmstadt, Germany) was used as a standard polysaccharide.

2.4. Hydrogen and carbon nuclear magnetic resonance (^1H and ^{13}C NMR)

^1H and ^{13}C NMR spectra of the HoPS were performed by NMR spectroscopy using a 400–MR NMR spectrometer (500 MHz, Agilent Technologies, California, USA). The sample (12 $mg.mL^{-1}$) was prepared in a NMR tube at 25 °C using deuterated dimethyl sulfoxide as solvent. Chemical shifts (δ) were expressed in ppm. ^{13}C NMR, distortionless enhancement by polarization transfer (DEPT-135), and heteronuclear single-quantum coherence (HSQC, 2D NMR) were conducted at 125 MHz and 70 °C. Data were processed using MestReNova software (Mestrelab Research S.L., Santiago de Compostela, Spain).

2.5. Conformational analysis

2.5.1. Congo red test

The test was carried out following the protocol described by Wang, Wang, Li, Zhang, You, Cheng, Luo and Zhang [17] with some modifications. HoPS solutions (2 $mg{\cdot}mL^{-1}$) were prepared in a gradient of NaOH solutions (0, 0.05, 0.1, 0.15, 0.2, 0.25, 0.3, 0.35, 0.4, 0.45 and 0.5 M) containing 0.35 μM Congo red. After 3 h reaction at 25 °C, the shifts

in the maximum visible absorption (λ_{max}) were recorded from 400 to 600 nm using an UV–visible spectrophotometer (Synergy HT – Biotek Instrument). Deionized water was used as negative control and commercial dextran was used as standard polysaccharide.

2.5.2. Circular dichroism (CD) spectroscopy

The CD spectra of the HoPS and the commercial dextran were recorded in a J-815 CD instrument (JASCO Corporation, Tokyo, Japan). The sample was prepared at 0.5 mg·mL^{-1} and measured in a quartz cuvette of 1 cm path length. The measurements were accumulated in the wavelength (λ) range of 200–400 nm with 100 nm·min^{-1} scanning speed, 2 s response, 1 nm bandwidth, and continuous scanning mode.

2.5.3. X-ray diffraction (XRD)

The XRD patterns of the purified HoPS and commercial dextran were recorded in a Bruker D8 Discover A 25 diffractometer (Bruker Corporation, Billerica, Massachusetts, USA) using CuKα radiation (λ = 1.5406 Å) and a silicon sample holder. The step size was 0.02°. The area measured the crystallinity index (CI) under crystalline peaks standardized ($A_{Crystal}$) with equivalent to total scattering area ($A_{Amorphous}$) using the following equation:

$$CI = \left(\Sigma A_{Crystal} / \Sigma A_{Crystal} + \Sigma A_{Amorphous}\right) \times 100$$

2.6. Hydrodynamic analysis

2.6.1. Determination of refractive index increment (dn/dC)

The dn/dc value was determined using a differential refractometer Brice-Phoenix BP-2000-V (Phoenix Precision Instrument Company, Pennsylvania, USA). The refractive index increment (dn) were analyzed with different HoPS solutions (dC) of 0.28, 0.57, 0.85, 1.13, 177 1.42 and 1.70 mg·mL^{-1} using Mili-Q water as solvent.

2.6.2. Static light scattering (SLS)

The weight average molar mass (MW) was measured by SLS at 25 °C employing a DAWN DSP photometer (Wyatt Technologies Corporation, California, USA) with a multiangle laser light scattering detector (λ = 632.8 nm). Different HoPS solution were prepared ranged between 0.01 and 1.00 mg·mL^{-1} using Milli-Q water as solvent. Solutions were subsequently filtered with a Millipore 0.22 μm filter before injection. The biopolymer MW was determined using the Astra software (Wyatt Technologies Corporation, California, USA).

2.6.3. Dynamic light scattering (DLS)

The hydrodynamic diameter (Dh) of the HoPS was analyzed by Zetaziser Nano ZS equipment (Malvern Panalytical Ltd., Worcestershire, UK) with a scattering angle of 173°. The HoPS sample (0.1 mg·mL^{-1}) was prepared in Mili-Q water at pH 5.7.

2.7. Coating characterization of the HoPS film on steel

2.7.1. Water and ionic contact angles (CA)

The CA measurement was carried out with a contact angle meter (DM-CE1; Kyowa Interface Science, Niiza, Saitama, Japan) equipped with a digital camera and image analysis software (FAMAS, Kyowa Interface Science, Niiza, Saitama, Japan). The HoPS film deposition was prepared by casting dropwise of polymer solution (1 g·L^{-1}) on the on stainless steel support (SS2343, Biolin Scientific, Suecia) and dried at 100 °C for 1 h on each drop aggregate. The advancing (A) and receding (R) angles were determined with a goniometer to observe a slight drop (2 μL) of Milli-Q® water and NaCl 5% solution placed on the biopolymer film after 40 s of exposition.

2.7.2. Atomic force microscopy (AFM)

A HoPS solution (1 g·L^{-1}) was prepared with Mili-Q water and 50 μL was uniformly dispersed on stainless steel support (SS2343, Biolin Scientific, Suecia) and dried at 100 °C with methanol fixation. AFM images were captured by scanning probe microscope (MultiMode 8-HR, Bruker, Massachusetts, USA) in tapping mode. Standard tapping mode was employed to determine the thickness of the polymer film using probe TESPA-V2 (Bruker, Massachusetts, USA) with nominal resonance frequency of 320 kHz and Force Constant of 42 N·m^{-1}. Images analysis was performed by Roughness routine Nanoscope Analysis 2.0 software (Bruker, Massachusetts, USA).

2.7.3. Electrochemical measurements

A carbon steel electrode (SAE 1020, area = 1 cm^2) was polished with grit paper in decreasing size from 180 to 2500 μm, followed by 0.3 μm alumina powder, and rinsed twice with distilled water. 200 μL of the HoPS sample (1 g·L^{-1}) was cast on a steel surface and heated at 100 °C for 1 h. Finally, it was rinsed and sonicated in tetrahydrofuran (Cicarelli Laboratories, Santa Fe, Argentina) to obtain functionalized steel coatings, hereafter called steel–HoPS. Electrochemical experiments were conducted with a Zahner IM6e potentiostat (ZAHNER-Elektrik GmbH & Co., Kronach, Germany). To evaluate the corrosion resistance of steel electrodes with and without the biopolymer layer, a single triangular potential sweep (STPS) between preset cathodic and anodic switching potentials was obtained at a potential scan rate of (v) = 0.020 V·s^{-1} was applied in a NaCl 5% solution. The potentiodynamic polarization curves were obtained at a scan rate of (v) = 0.001 V·s^{-1}. A standard three-electrode cell with a large area Pt sheet counter electrode and a saturated calomel reference electrode (SCE) was used. All the potentials were referred to the SCE [0.241 V vs. standard hydrogen electrode (SHE)]. Experiments were done at 25 °C. Electrochemical impedance spectroscopy (EIS) measurements were carried out at open circuit potential (OCP) by producing a small amplitude sinusoidal perturbation (10 mV peak-to-peak) in the 30 kHz ≥ f ≥ 10 mHz frequency range, with f = ω·2π^{-1}. Finally, the electrodes (bare steel and the stell-HoPS) were subsequently characterized by SEM and EDS before and after the electrochemical test. Both techniques belong to facilities of INBIONATEC-UNSE-CONICET CCT NOA Sur, Argentina.

2.8. Statistical analysis

Assays were performed with two repetitions ($n = 2$). The ANOVA test (one-way) determined statistical significance, and significant differences by post-hoc analysis using Tukey-HSD at $P < 0.05$ (Infostat, Córdoba, Argentina).

3. Results and discussion

3.1. HoPS production and purification

W. cibaria FMy 2-21-1 is a LAB strain capable of producing an α-glucan with multiple techno-functional applications for the food industry [11]. In our trial, its HoPS production was 4.82 g·kg^{-1}, which was similar to that reported for other *Weissella* strains under similar fermentation conditions [11,18]. No precipitate was observed after centrifuging the cold solution (5 mg·mL^{-1}) and the Bradford assay did not detect protein. The UV spectra showed one single peak between 190 and 210 nm, typical for carbohydrates (Fig. S1, in Supporting Information). The lack of signals at 260, 280, and 400 nm indicated the absence of proteins, nucleic acids, and pigments in the sample, respectively [19].

3.2. Structural characterization

FT-R spectra of the HoPS and commercial dextran (Fig. 1**A** and Table S1 in Supporting Information) were performed to investigate their chemical structures (functional groups, glycosidic linkages, etc.) based on the detection of vibrations through electrical polarizability changes [20]. The intense band around 2912 cm^{-1} corresponds to the pyranoid

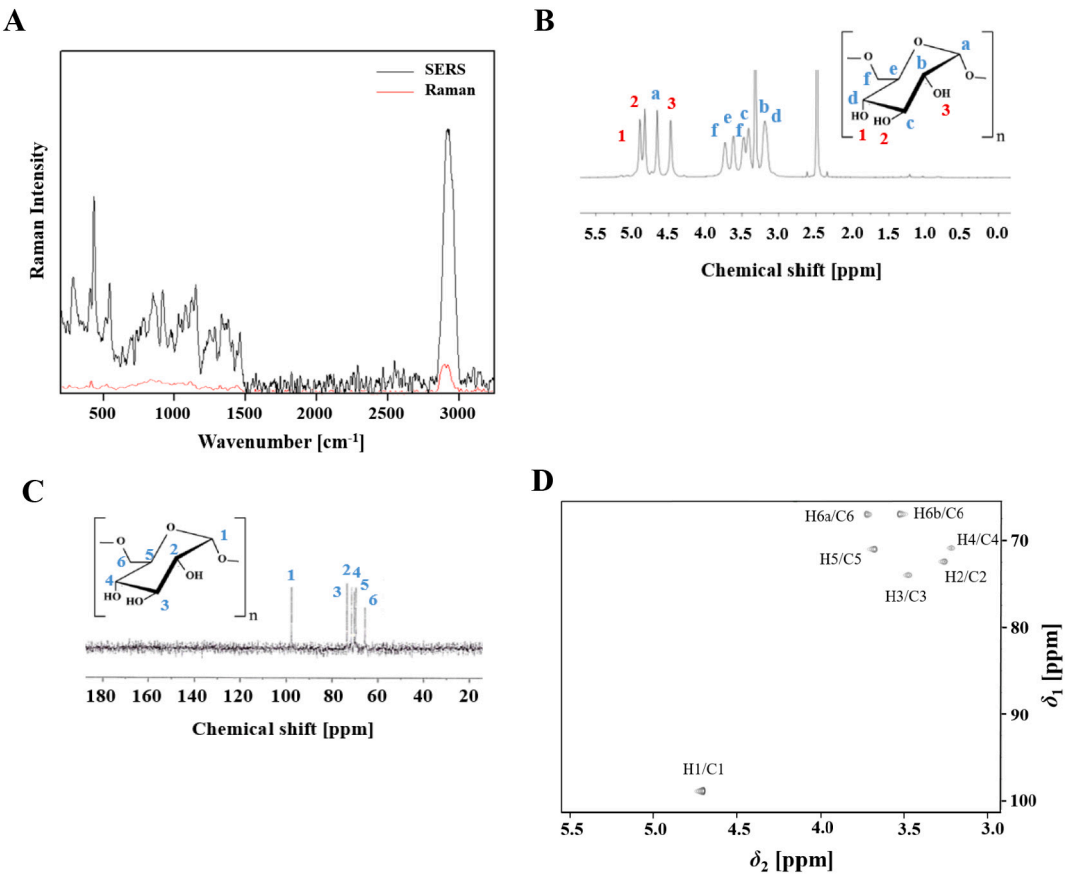

Fig. 1. Structural analysis of the purified HoPS produced by *Weissella cibaria* FMy 2–21-1 strain. Specific spectroscopic profiles corresponded to the applied methodology. **A.** FT-Raman and SERS. **B.** ^{1}H NMR. **C.** ^{13}C NMR. **D.** HSQC.

ring's C—H stretching vibration, commonly in glucan polymer [21]. No signals between 1750 and 1540 cm^{-1} corresponding to acidic groups [22] were observed, confirming the neutral nature of the polysaccharide as reported by Lobo et al. [11]. The region 1500–1200 cm^{-1} is assigned principally to vibrational modes of C—H, CH_2, C—C—H, O—C—H, and C—OH deformations. The deforming mode of methylene groups (CH_2), typical of dextran, appears around 1442 cm^{-1}. On the other hand, the moderate-intensity signals between 1370 and 1330 cm^{-1} are modes involving considerable coupling of bendings between C—H with some H—C—C and C—O—H deformations [20,23]. The C—O stretching with contributions of C—C vibrations (ring mode) and glycosidic bonds appear in 1200–950 cm^{-1}. Signals around 1146, 1116, and 1064 cm^{-1} are characteristic of symmetric stretching from C—O—C linkages [22,24]. Signals into 950–700 cm^{-1} are commonly known as the anomeric region, containing weak bands of C—H linkage deformation sensitive to glucose conformers in glycosidic bonds (α or β). The bands between 850–840cm^{-1} and 785–765 cm^{-1} are characteristic of α-D anomer in dextran polymer. However, the absence of signals between 890 and 870 cm^{-1} evinced that the HoPS structure lacks β-linkages [25]. Vibrations below 700 cm^{-1} are distinctive for many polysaccharides, and these are often sensitive to the deformation of skeletal modes of pyranose rings, dihedral angles of the glycosidic linkages, and the nonplanar bending of —OH groups [26,27].

SERS can significantly enhance the FT-R signals if the sample is attached or close to nanometer-roughened metal (Ag, Au, or Cu) surfaces [28]. Fig. 1A and Table S1 show the SERS methodology application results in the HoPS solution using AgNPs (Fig. S3). The AgNPs UV spectrum (Fig. S3A) exhibited an absorption band around 400 nm corresponding to the surface plasmon resonance of the conducting electrons on the nanoparticle surface. SEM images showed sizes between 40 and 80 nm with some aggregates between 130 and 180 nm (Fig. S3B and C). The Ag elemental in the nanoparticle structure was also evidenced by EDS at 3.1 Kev (Fig. S3D). These results agreed with previous reports [29,30]. The most significant signals in the SERS spectrum (Table S1), not observed by FT-R, include bands around the 1378 cm^{-1} corresponding to C—H bending with some O—H contribution. Signals at 1284 and 1075 cm^{-1} are involved in D-glucosidic bonds coupled with C—OH stretching [31,32]. A dextran structure signal was evidenced with the band at 912 cm^{-1} attributed to α-(1, 6) linkages by the rotational isomerism of elementary links caused by rotation about the C_1—O_1, C_6—O_6, and C_6—C_5 linkages [33]. Bands around 544 cm^{-1} were due to C_4—C_5—O vibrations of the glucopyranose ring coupling with C_1—O_6—C_6 of the glycosidic bond [34,35]. Finally, the peak at 406 cm^{-1} corresponded to the C—C—O in-plane deformation of α–glucose [23].

NMR spectroscopy is a powerful tool for obtaining detailed information about the glycosidic bond configurations and the repetitive unit sequences of the polysaccharide chain. ^{1}H and ^{13}C NMR spectra of the biopolymer are shown in Fig. 1B and C. The chemical shifts from δ 3.0 to 3.8 ppm and δ 4.3 to 5.0 ppm in the ^{1}H NMR spectrum (Fig. 1B) were assigned to protons of carbon rings and hydroxyl groups dextran structure [36,37]. The anomeric signal at 4.83 ppm was typical of D-glucosyl residues α-(1,6)-linked in the dextran backbone. No other signals were recorded in the anomeric region, indicating the absence of branching linkages. The intense peaks at 2.48 and 3.31 ppm corresponded to DMSO and traces of water in the HoPS simple. The ^{13}C NMR spectrum (Fig. 1**C**) shows the α-anomeric (C_1) carbon at 97.8 ppm, while the ring carbon 283 signals were at 71.5, 73.5, 70.3, and 69.7 (C_2, C_3, C_4, and C_5, respectively). The downfield shift of the C_6 carbon signal for the glucose monomer at 65.60 ppm evidenced the α-(1, 6) linkages in the HoPS structure. These results are in agreement with Bratuša et al. [38]. No additional peak was observed in the 75–85 ppm region, indicating the

absence of branched linkages [39]. The chemical shifts of carbons in the DEPT-135 spectrum (Fig. S4) showed five signals of the methine group (CH) referring to C_1, C_2, C_3, C_4, and C_5 (δ 97, 72, 74, 69, and 70 ppm, respectively) and one signal of a methylene group (CH_2) at δ 66 ppm (C_6). The HSQC spectrum (Fig. 1D) showed the correlation between ^1H and ^{13}C direct bonds. Seven protons correlate typically to glucose residue with the correlation between ^1H at 4.68 ppm and ^{13}C at 98.87 ppm, confirming the presence of α-(1,6) glycosidic bond. Other assignments from the HSQC analysis of each position are represented in Table S2. The absence of signals between δ 4.4–4.8 ppm and δ 101–105 ppm in ^1H and ^{13}C NMR, respectively, confirmed the absence of β configuration in the HoPS structure [40,41]. Thus, the NMR studies concluded that the biopolymer structure produced by *W. cibaria* FMy 2-21-1 is an unbranched dextran formed by α-(1, 6)-D glucosyl residues similar to dextran produced by *W. cibaria* CMU and *W. cibaria* DSRWC [42,43].

3.3. Conformational analysis

Congo red is an azo dye that can form a complex with polysaccharides possessing a triple-stranded helical conformation in weakly alkaline conditions generating a bathochromic shift λ_{max} compared to Congo red spectrum [44]. Fig. 2A shows λ_{max} changes of Congo red, Congo red–HoPS, and Congo red–commercial dextran in different NaOH concentrations. The bathochromic shift values were not observed in all experiments at all alkaline concentrations indicating that both biopolymers adopt a random coil conformation in aqueous solutions rather than helicoidal. These results agreed with the biopolymers' structures reported from other LAB strains [44,45]. The side-chain interaction significantly affects random coil conformation and often constitutes enzyme active sites and other protein-specific functional sites. Besides, the conformational entropy generated significantly contributes to its energetic stabilization [44].

CD analysis is an effective method for exploring the polysaccharide chain conformation [45]. CD spectra of the purified HoPS and commercial dextran ranging from 200 nm to 400 nm are represented in Fig. 2B. Both spectra exhibited some different ellipticity bands. The HoPS spectrum showed strong positive Cotton effects around 203 nm and 218 nm, while the commercial polysaccharide spectrum exhibited a negative band around the latter one. These results suggest that the HoPS presents an asymmetric conformation than commercial dextran, probably due to branching linkage presence (commercial dextran have ~5% of branching) or hydrogen-bond interactions that could affect the chirality of their sugar rings. Also, Fig. 2B showed a significant redshift at 254 nm with subsequent decreasing intensity until 400 nm for both biopolymers. Similar results were reported in [44,45].

The semi-crystalline nature of polysaccharides is key to forming polymeric films [46]. XRD was used to characterize the distribution phase of polysaccharides' amorphous and crystalline nature [47]. The XRD spectra of purified HoPS and commercial dextran are represented in Fig. 2C, recorded between the angles (2θ) 0° to 70°. Both diffractograms exhibited the same profile, suggesting a similar crystalline nature. These polymer spectra present broad bands around 18.50°, 22.2°, and 42.3° indicating amorphous components. However, the XRD patterns revealed a low overall crystallinity confirming a semi-crystalline structure in both samples (CI: 25.6% and 20.8% for the HoPS and commercial dextran, respectively). These results were consistent with the crystallinity of the biopolymer (CI: 23.0%) produced by *W. confusa* KR780676 [46].

3.4. Hydrodynamic analysis

Some hydrodynamic parameters (dn/dC, MW, and R_H) of the purified HoPS were studied to understand the relationships between the primary structure and spatial conformation in aqueous solutions. The specific dn/dC increment is essential to determine the average MW and the molecular size of the HoPS by light scattering techniques [48]. The

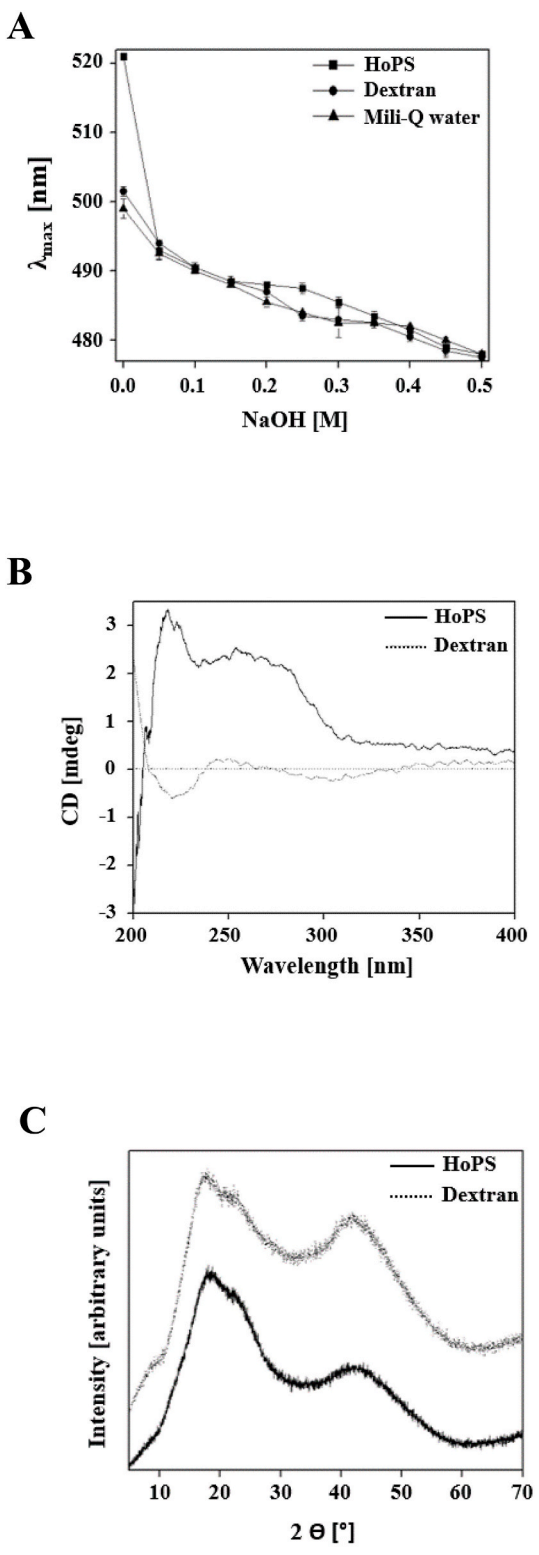

Fig. 2. Molecular conformation and crystallinity index of the purified biopolymer. **A.** Variation in λ_{max} for the complexes formed by Congo red with HoPS and commercial dextran at different NaOH concentrations. Mili Q-water was used as the negative control. **B.** CD spectrum of HoPS and commercial dextran in the range of 200–400 nm at 25 °C. **C.** XRD spectra of HoPS and commercial dextran.

dn/dC index determined for HoPS solutions resulted in 0.13 $mL{\cdot}g^{-1}$ which is a typical value for polysaccharides (~0.14 $mL{\cdot}g^{-1}$) [49]. The SLS and DLS analysis are combined to provide quali and quantitative information about the macromolecular architecture. The SLS technique can determine the MW, the mean-square radius of gyration (Rg), and the second virial coefficient (A_2) using the Zimm-plots equation [50]. The Zimm plot of the HoPS solutions is shown in Fig. 3A. The MW, R_g, and A_2 parameters were obtained after two extrapolations: $q^2 \rightarrow 0$ (q, scattering vector) and $C \rightarrow 0$ (C, polymer concentration) [51], resulting in 7670 kDa, 377.73 nm, and $3.415.10^{-6}$ $mL{\cdot}mol{\cdot}g^{-2}$, respectively. These results show that the biopolymer exhibited high MW and Rg in water solution, influencing the previous outcome (Fig. 2B). On the other hand, the positive A_2 value suggests highly favorable molecular interactions between the solvent and the HoPS. Similar results were observed by Exarhopoulos, Raphaelides and Kontominas [49] for a kefiran polysaccharide.

DLS relies on the translational diffusion coefficient of the molecules' measure, which is related to their size using relevant theoretical relations [52]. Size distribution by intensities and the autocorrelation functions obtained from DLS are exhibited in Fig. 3B and Fig. S5. DLS analysis of the biopolymer showed uniform distribution of particles with R_H = 214 nm, and the polydispersity index (PI) was 0.44, similar to results obtained for commercial dextran T10 (PI = 0.42) reported by Bund, Allelein, Arunkumar, Lucey, and Etzel [53]. The combination of R_g and the calculated R_H was used to obtain the ρ coefficient necessary to infer the polymer conformation. The ρ value was 1.7, corresponding to random coil conformation in water [49], in agreement with previous results (Fig. 2A).

3.5. Biocoating studies

AFM is routinely used to construct images with nanometer resolution, by rastering a small tip mounted on a cantilever across the sample surface [3]. AFM imaging of the biopolymer film on a steel wafer showed an overall thickness of 587 nm when measuring the depth of a scratch on the coating (Fig. S6). Topographical images (Fig. 4) exhibited many spherical and irregular lumps enclosed in the whole platform, which looked like grainy networks (Fig. 4A and B). The maximum height

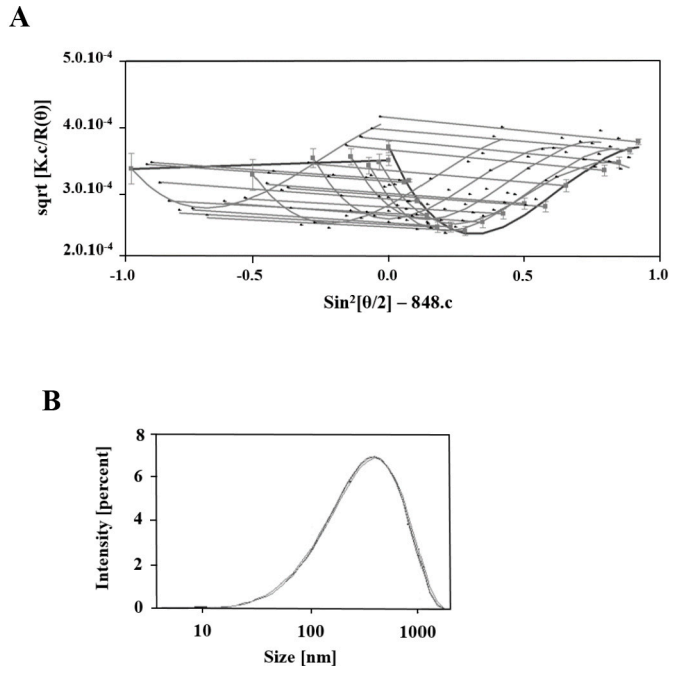

Fig. 3. SLS and DLS applications of the purified HoPS in aqueous solutions. **A.** Zimm plot. **B.** Size distribution.

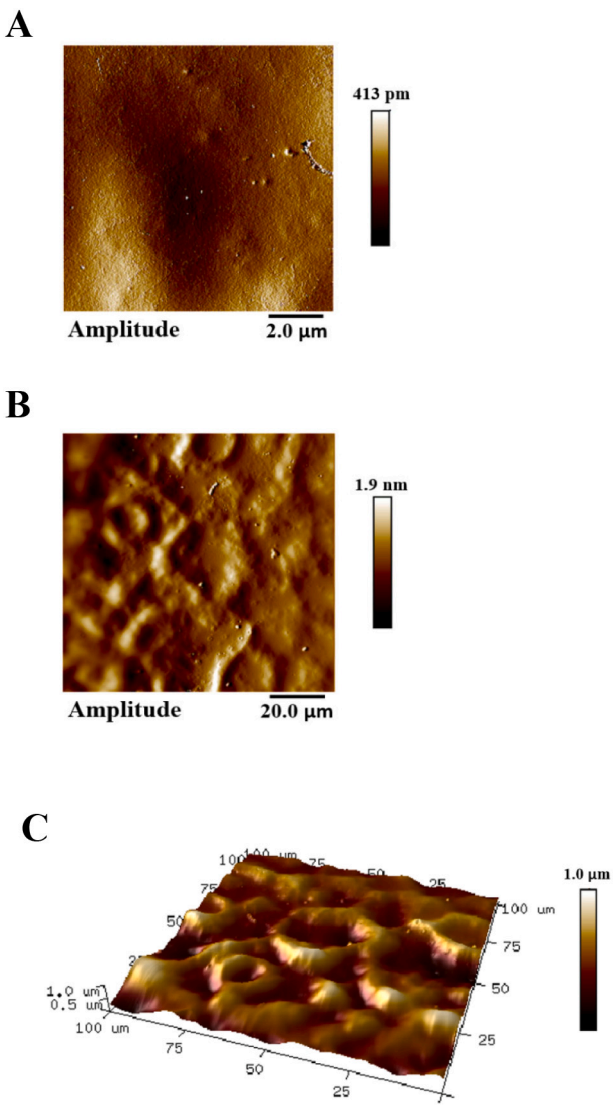

Fig. 4. AFM images of the steel-HoPS film. **A.** and **B.** Planar images scanned at different magnification levels. **C.** 3 D image.

of single spherical lumps was 290 nm, and surface roughness was 1.19 µm. Hence, this biopolymer-packed form presented an affinity which was solid enough to cover steel surface (Fig. 4**C**). Furthermore, Lobo et al. [11] discovered that the polymer under study showed a cubic-grump morphology, when they observed it under a SEM microscope. Similar lump types were observed for other LAB glucans [46,47].

Water CA measurement is a valuable parameter to characterize the HoPS films on surfaces. The CA formed by droplets slowly expanding over a surface and contracting along its previous path is called advancing (A) and receding (R), respectively. Angles which are smaller than 90° correspond to hydrophilic surfaces, while those greater than 90° correspond to hydrophobic ones [54]. Fig. S7 shows that the surface coated with HoPS revealed hydrophilic features: A51.8° and R50.4°. Nonetheless, it turned out to be more hydrophobic than the bare surface itself: A18.5° and R18.8°. The R angle was lower than the A angle, because the biopolymer coating absorbed moisture, resulting in a swelling coating film [3]. The coating became more hydrophobic in ionic environments than in water (A55.8° and R55.0°). Similar results were observed by Finkenstadt, Bucur, Côté, and Evans [3] for comparable biopolymer films.

The casting of aqueous coatings brought the metal into direct contact with water in the polymer solution. Film formation depended upon

water evaporation, polymer coalescence, and adherence to metal surface [12]. After heating the coating solution for 1 h to functionalize it on bare steel, the HoPS heteroatoms (O) of its functional groups were adsorbed on the steel surface, while displacing water molecules that formed complexes with metal ions all over the surface [8,12]. SEM images (Fig. 5A and C) directly show the surface topographical differences of bare steel and the steel coated by HoPS, respectively. The HoPS covered the entire surface of the metal homogeneously since no metallic elements were observed by the EDS analysis in different point sets of the sample surface (Fig. S8A and B). The electrochemical behavior of the steel-HoPS film (Fig. 6) gave information about the effectiveness of its functionalization against corrosive aqueous media containing chloride ions. The anodic behavior of the biopolymer film was analyzed by cyclic voltammetry within the $-0.7\ V < E < 0.0\ V$ potential range (Fig. 6A). In the anodic excursion, bare steel exhibited a current plateau corresponding to the passive region, due to oxide formation at $E > -0.40\ V$. This sudden increase in current was associated with passivity breakdown, induced by the aggressive Cl^- anions and subsequent pitting corrosion (Fig. S9). The passivation potential for the pits was recorded at -0.58 V. Steel corrosion began with anodic oxidation of Fe to Fe^{2+}. Fe^{2+} underwent further oxidation to Fe^{3+}, which then accelerated the conversion of Fe to Fe^{2+} [12]. The behavior of the steel-HoPS system was different within the same potential range previously discussed. No pitting processes were visible in the steel-HoPS surfaces. The charge in the anodic peak was higher than in the cathodic scan (Fig. S9), indicating that the steel underwent some corrosion through the oxide layer during the anodic process and oxide formation. However, the current density in the broad potential range was smaller than that recorded for the steel sample, in accordance with Moradi, Song, and Xiao [8] findings. This difference is exposed in the topographical surfaces of both electrodes (Fig. 5B and D). The adherence of HoPS films to metal surfaces could significantly alter the redox potential of Fe Fe^{2+}/Fe^{3+} [8,12]. It is important to remark that the biofilm remains attached to the metal surface after the electrochemical test (Fig. S8C and D).

Polarization curves (Fig. 6B) helped determine corrosion rate and the reaction mechanism (anodic, cathodic, or both) [3]. Fig. 6B shows the experimental Tafel plots of bare steel and steel–HoPS analyzed in the $-0.7\ V < E < -0.2\ V$ potential range. The corrosion of the unprotected bare metal occurs at higher currents than the coated steel. Consequently,

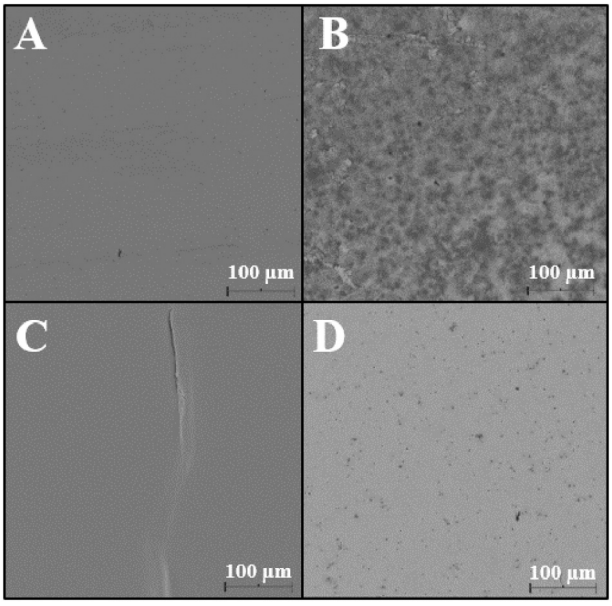

Fig. 5. SEM images of the corrosion process of bare steel and coated steel substrates. ***A.*** *Bare* steel. **B.** bare steel after the corrosion process. **C.** Steel-HoPS. **D.** Steel-HoPS after the corrosion process.

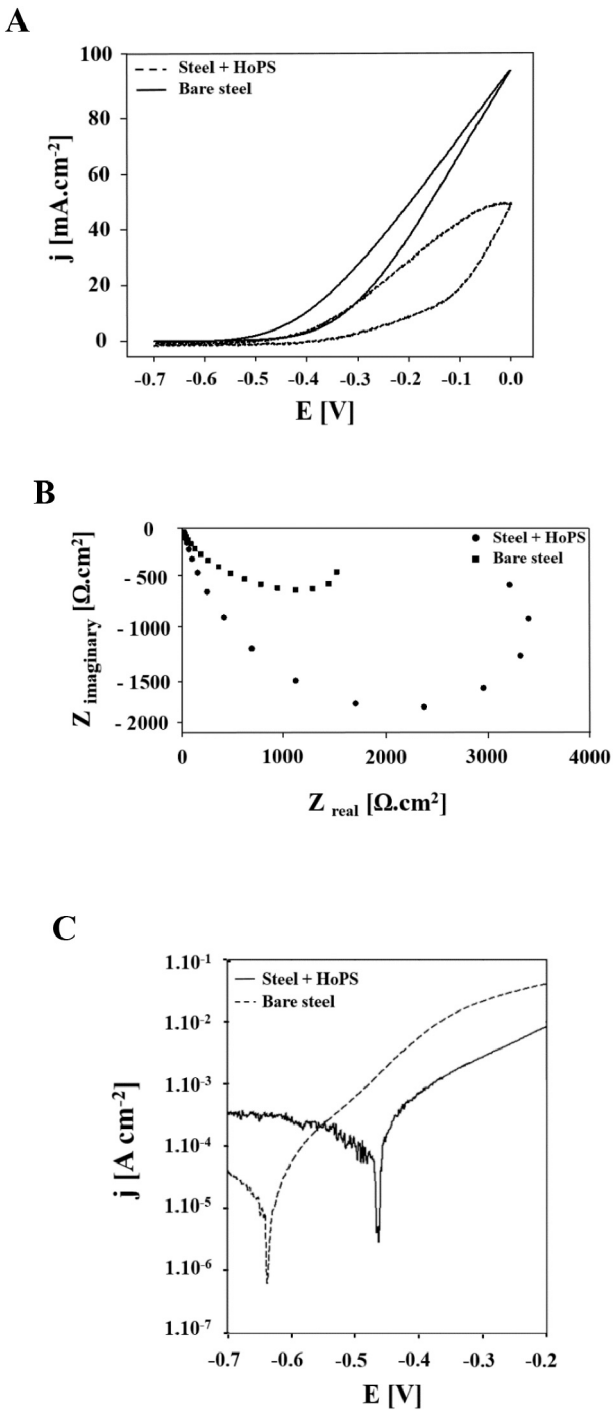

Fig. 6. Electrochemical analysis in an ionic environment (NaCl 5%). **A.** Cyclic voltammograms. **B.** Polarization curve. **C.** Nyquist plots.

the anodic reaction was reduced by the HoPS coating, with the open corrosion potential tending to shift towards less negative values. The abovementioned findings suggest that the biopolymer produced by the *W. cibaria* strain acted predominantly as an anodic-type corrosion inhibitor. Exopolysaccharide coatings could inhibit corrosion by: (i) forming a protective barrier between the metal substrate and the corrosive environment (salt solution), and slowing down the diffusion of corroding species through the coating; and (ii) adhering to the metal surface and reacting with it to create a passive layer, thus blocking the corroding species from the surface [3]. Moreover, Finkenstadt et al. [3] reported similar results for dextrans produced by *Liquorilactobacillus*

satsumensis and *Leuconostoc citreum* strains under similar corrosion conditions using SAE 1010 stainless steel as support.

EIS was used to compare the behavior of the two surfaces in chloride-containing solutions at open circuit potential. Fig. 6**C** showed the experimental Nyquist plots of steel and steel-HoPS coating exhibiting a single well-defined semicircle covering the whole range of frequencies for both systems. The high polarization resistance of steel-HoPS (R_{Pol} ~ 3500 Ω·cm^2) concerning steel (R_{Pol} ~ 1500 Ω·cm^2) confirmed that the biocoating provided a protective layer for steel electrodes. Therefore, such behavior suggests that this bright coating reduces ion diffusion processes, and it can reduce the rate of corrosion of the substrate, in agreement with what was reported in previous works (Fig. 6A). Moreover, the steel-HoPS Nyquist plot indicated that the biopolymer layer decreased water and ions access and their subsequent adsorption on the steel surface, thus hindering oxide film formation in the anodic process. Similar impedance effects were observed for the following biocoatings: levan L0406 from *Bacillus* sp., and dextrans produced by *Liquorilactobacillus satsumensis* NRRL B-1254 and *Leuconostoc citreum* NRRL B-1498 strains in chloride-containing solutions [3,12]. On the other hand, the Bode plot (Fig. S10) for bare steel showed a maximum φ value of 63° for the first time constant, which could be associated with the oxide film formed on the metal surface during the corrosion process. Furthermore, the presence of the HoPS on the steel caused an increase in the value of maximum φ concerning steel (72°). This demonstrated that the biopolymer protected the steel surface by minimizing corrosion, thus confirming previous findings (Fig. 6).

4. Conclusion

From the point of view of green chemistry, LAB HoPS are promising natural products from renewable sources, which are capable of replacing synthetic, toxic, and expensive commercial anticorrosives. According to previous literature, *W. cibaria* FMy 2-21-1 produces enough extracellular glucans in sucrose enriched media, which can be recovered without impurities and which exhibit FT-R vibrational profiles similar to those of commercial dextrans. The SERS spectrum (enhanced with AgNP) was a complementary tool for characterizing HoPS since it revealed new signals of the polymer structure, mainly related to α-(1,6) linkages. On the other hand, all the NMR experiments confirmed the classification of the studied biopolymer as a dextran type with a linear backbone of consecutive α-(1,6)-linked D-glucopyranose units, with no branching. Furthermore, the HoPS showed an extended molecular conformation in solutions, with strong polymer interactions and significant molecular weight and size. On the other hand, the HoPS coating adhered homogeneously to the steel surface, revealing a packed forming grainy network. This biocoating exhibited a hydrophilic character in aqueous and ionic environments, but it had a more hydrophobic role under ionic conditions. Heat functionalization of metal surface through heteroatoms (O) allowed the steel-HoPS system to reduce the transport of current density by cyclic voltammetry. The above hinders the formation of oxide deposits that pitting rust normally triggers, as observed in topographical images. Moreover, as suggested by the Tafel plots, the biocoating acted as an anodic-type corrosion inhibitor. Furthermore, the HoPS film reduced water and ions diffusion on the metal surface, by increasing the overall impedance showed by EIS. Research in the biotechnological production of the HoPS, the film formation kinetics of this polymer at different concentrations, the dynamics of water and ionic diffusion through its coating, as well as its adsorption and chelation onto metal surface, is currently underway for a deeper knowledge of its anticorrosive potential.

CRediT authorship contribution statement

René Emanuel Lobo: Conceptualization, Methodology, Validation, Formal analysis, Investigation, Data curation, Writing – original draft, Writing – review & editing. **Patricio Andrés Orrillo:** Investigation, Formal analysis, Data curation, Writing – original draft, Writing – review & editing. **Susana Beatriz Ribotta:** Funding acquisition, Investigation, Formal analysis, Resources. **Graciela Font de Valdez:** Resources, Writing – review & editing. **Mercedes Santos García:** Methodology, Validation, Formal analysis, Investigation, Writing – original draft. **José Carlos Rodríguez Cabello:** Investigation, Supervision, Resources, Writing – review & editing. **María Inés Torino:** Funding acquisition, Conceptualization, Supervision, Project administration, Writing – review & editing.

Acknowledgments

We thank Dr. Mozzi for providing the *Weisella* strain and the following fundings: PICT 1705 (ANPCyT–FONCyT, Argentina), PID2019-110709RB-100, RTI2018-096320-B-C22, RED2018-102417-T (Spanish Government), VA317P18, Infrared2018-UVA06 (Junta de Castilla y León), 0624_2IQBIONEURO_6_E (Interreg V España Portugal POCTEP) and Centro en Red de Medicina Regenerativa y Terapia Celular de Castilla y León. Finally, we are also grateful to Prof. Manes A. for their corrections pertaining to the English language.

Appendix A. Supplementary data

Supplementary data to this article can be found online at https://doi.org/10.1016/j.ijbiomac.2022.05.105.

References

[1] M. Basik, M. Mobin, M. Shoeb, Cysteine-silver-gold nanocomposite as potential stable green corrosion inhibitor for mild steel under acidic condition, Sci. Rep. 10 (1) (2020) 1–12.
[2] Y. Sushmitha, P. Rao, Material conservation and surface coating enhancement with starch-pectin biopolymer blend: a way towards green, Surf. Interfaces 16 (2019) 67–75.
[3] V.L. Finkenstadt, C.B. Bucur, G.L. Côté, K.O. Evans, Bacterial exopolysaccharides for corrosion resistance on low carbon steel, J. Appl. Polym. Sci. 134 (29) (2017) 45032.
[4] B. Charitha, P. Rao, Pullulan as a potent green inhibitor for corrosion mitigation of aluminum composite: electrochemical and surface studies, Int. J. Biol. Macromol. 112 (2018) 461–472.
[5] L. Muthulakshmi, B.A. Kumar, A. Rajasekar, J. Annaraj, C.I. Pruncu, The benefits of k-carrageenan-gelatin hybrid composite coating on the medical grade stainless steel (SS304) used as anticorrosive barrier, Mater. Chem. Phys. 258 (2021), 123909.
[6] J. Scheerder, R. Breur, T. Slaghek, W. Holtman, M. Vennik, G. Ferrari, Exopolysaccharides (EPS) as anti-corrosive additives for coatings, Prog. Org. Coat. 75 (3) (2012) 224–230.
[7] A. Alipour, A. Bahrami, E. Saebnoori, Investigation in effect of different culture medium on the anti-corrosive performance of bacterial biopolymer, J. Taiwan Inst. Chem. Eng. 77 (2017) 64–72.
[8] M. Moradi, Z. Song, T. Xiao, Exopolysaccharide produced by *Vibrio neocaledonicus* sp. as a green corrosion inhibitor: production and structural characterization, J. Mat Sci. Technol. 34 (12) (2018) 2447–2457.
[9] M. Khani, A. Bahrami, M.D. Ghafari, Optimization of operating parameters for anti-corrosive biopolymer production by *Chryseobacterium indologenes* MUT. 2 using central composite design methodology, J. Taiwan Inst. Chem. Eng. 59 (2016) 165–172.
[10] P.G. Cataldo, J. Villena, M. Elean, G.S. de Giori, L. Saavedra, E.M. Hebert, Immunomodulatory properties of a γ-aminobutyric acid-enriched strawberry juice produced by *Levilactobacillus brevis* CRL 2013, Front. Microbiol. 11 (2020) 11: 610016.
[11] R.E. Lobo, T. Figueroa, D. Navarro, M.I. Gómez, G.F. de Valdez, M.I. Torino, Techno-functional properties of HoPS from lactic acid bacteria of different origins as potential food additives, Food Chem. 356 (2021), 129627.
[12] V.L. Finkenstadt, G.L. Côté, J. Willett, Corrosion protection of low-carbon steel using exopolysaccharide coatings from *Leuconostoc mesenteroides*, Biotechnol. Lett. 33 (6) (2011) 1093–1100.
[13] M. Miao, Y. Ma, C. Huang, B. Jiang, S.W. Cui, T. Zhang, Physicochemical properties of a water soluble extracellular homopolysaccharide from *Lactobacillus reuteri* SK24. 003, Carbohydr. Polym. 131 (2015) 377–383.
[14] L.d.Y. Pozzo, T.F. da Conceição, A. Spinelli, N. Scharnagl, A.T. Pires, Chitosan coatings crosslinked with genipin for corrosion protection of AZ31 magnesium alloy sheets, Carbohydr. Polym. 181 (2018) 71–77.
[15] R.E. Lobo, M.I. Gómez, G.F. de Valdez, M.I. Torino, Physicochemical and antioxidant properties of a gastroprotective exopolysaccharide produced by *Streptococcus thermophilus* CRL1190, Food Hydrocoll. 96 (2019) 625–633.

[16] P. Lee, D. Meisel, Adsorption and surface-enhanced Raman of dyes on silver and gold sols, J. Phys. Chem. 86 (17) (1982) 3391–3395.
[17] K.-P. Wang, J. Wang, Q. Li, Q.-L. Zhang, R.-X. You, Y. Cheng, L. Luo, Y. Zhang, Structural differences and conformational characterization of five bioactive polysaccharides from *Lentinus edodes*, Food Res. Int. 62 (2014) 223–232.
[18] S. Galle, C. Schwab, E. Arendt, M. Gänzle, Exopolysaccharide-forming *Weissella* strains as starter cultures for sorghum and wheat sourdoughs, J. Agric. Food Chem. 58 (9) (2010) 5834–5841.
[19] X.-W. Li, S. Lv, T.-T. Shi, K. Liu, Q.-M. Li, L.-H. Pan, X.-Q. Zha, J.-P. Luo, Exopolysaccharides from yoghurt fermented by *Lactobacillus paracasei*: production, purification and its binding to sodium caseinate, Food Hydrocoll. 102 (2020), 105635.
[20] I.H. Boyaci, H.T. Temiz, H.E. Geniş, E.A. Soykut, N.N. Yazgan, B. Güven, R. S. Uysal, A.G. Bozkurt, K. İlaslan, O. Torun, Dispersive and FT-Raman spectroscopic methods in food analysis, RSC Adv. 5 (70) (2015) 56606–56624.
[21] K. Nowak, A. Wiater, A. Choma, D. Wiącek, A. Bieganowski, M. Siwulski, A. Waśko, Fungal (1→3)-α-d-glucans as a new kind of biosorbent for heavy metals, Int. J. Biol. Macromol. 137 (2019) 960–965.
[22] N.P. Ivleva, M. Wagner, H. Horn, R. Niessner, C. Haisch, Towards a nondestructive chemical characterization of biofilm matrix by Raman microscopy, Anal. Bioanal. Chem. 393 (1) (2009) 197–206.
[23] M. Tahir, M.I. Majeed, H. Nawaz, S. Ali, N. Rashid, M. Kashif, I. Ashfaq, W. Ahmad, K. Ghauri, F. Sattar, Raman spectroscopy for the analysis of different exo-polysaccharides produced by bacteria, Spectrochim. Acta A Mol. Biomol. Spectrosc. 237 (2020), 118408.
[24] E. Wiercigroch, E. Szafraniec, K. Czamara, M.Z. Pacia, K. Majzner, K. Kochan, A. Kaczor, M. Baranska, K. Malek, Raman and infrared spectroscopy of carbohydrates: a review, <sb:contribution><sb:title>Spectrochim. Acta A Mol. Biomol</sb:title></sb:contribution><sb:host><sb:issue><sb:series><sb:title>Spectrosc.</sb:title></sb:series></sb:issue></sb:host> 185 (2017) 317–335.
[25] S.-N. Yuen, S.-M. Choi, D.L. Phillips, C.-Y. Ma, Raman and FTIR spectroscopic study of carboxymethylated non-starch polysaccharides, Food Chem. 114 (3) (2009) 1091–1098.
[26] M. Chylińska, M. Szymańska-Chargot, A. Zdunek, FT-IR and FT-Raman characterization of non-cellulosic polysaccharides fractions isolated from plant cell wall, Carbohydr. Polym. 154 (2016) 48–54.
[27] B. Matsuhiro, I.O. Osorio-Román, R. Torres, Vibrational spectroscopy characterization and anticoagulant activity of a sulfated polysaccharide from sea cucumber *Athyonidium chilensis*, Carbohydr. Polym. 88 (3) (2012) 959–965.
[28] R.S. Das, Y. Agrawal, Raman spectroscopy: recent advancements, techniques and applications, Vib. Spectrosc. 57 (2) (2011) 163–176.
[29] E. de Barros Santos, N.V. Madalossi, F.A. Sigoli, I.O. Mazali, Silver nanoparticles: green synthesis, self-assembled nanostructures and their application as SERS substrates, New J. Chem. 39 (4) (2015) 2839–2846.
[30] P. Liou, F.X. Nayigiziki, F. Kong, A. Mustapha, M. Lin, Cellulose nanofibers coated with silver nanoparticles as a SERS platform for detection of pesticides in apples, Carbohydr. Polym. 157 (2017) 643–650.
[31] M. Mathlouthi, J.L. Koenig, Vibrational spectra of carbohydrates, in: R.S. Tipson, D. Horton (Eds.), Advances in Carbohydrate Chemistry And Biochemistry, Elsevier, Amnsterdam, 1987, pp. 7–89.
[32] D.C. Siew, R.P. Cooney, M.J. Taylor, P.M. Wiggins, Vibrational spectroscopic studies of aqueous dextran sulphate, J. Raman Spectrosc. 25 (7–8) (1994) 727–733.
[33] R. Zhbankov, V. Andrianov, M. Marchewka, Fourier transform IR and Raman spectroscopy and structure of carbohydrates, J. Mol. Struct. 436 (1997) 637–654.
[34] A. Synytsya, M. Novak, Structural analysis of glucans, Ann. Transl. Med. 2 (2) (2014) 17.
[35] R. Zhbankov, S. Firsov, E. Korolik, P. Petrov, M. Lapkovski, V. Tsarenkov, M. Marchewka, H. Ratajczak, Vibrational spectra and the structure of medical biopolymers, J. Mol. Struct. 555 (1–3) (2000) 85–96.
[36] D. Ikkene, A.A. Arteni, H. Song, H. Laroui, J. Six, K. Ferji, Synthesis of dextran-based chain transfer agent for RAFT-mediated polymerization and glyco-nanoobjects formulation, Carbohydr. Polym. 234 (2020), 115943.
[37] H. Lian, Y. Du, X. Chen, L. Duan, G. Gao, C. Xiao, X. Zhuang, Core cross-linked poly (ethylene glycol)-graft-dextran nanoparticles for reduction and pH dual responsive intracellular drug delivery, J. Colloid Interface Sci. 496 (2017) 201–210.
[38] A. Bratuša, T. Elschner, T. Heinze, E. Fröhlich, S. Hribernik, M. Božič, E. Žagar, K. S. Kleinschek, M. Thonhofer, R. Kargl, Functional dextran amino acid ester particles derived from N protected S-trityl-L-cysteine, Colloids Surf. B: Biointerfaces 181 (2019) 561–566.
[39] G. Ye, Y. Chen, C. Wang, R. Yang, X. Bin, Purification and characterization of exopolysaccharide produced by *Weissella cibaria* YB-1 from pickle Chinese cabbage, Int. J. Biol. Macromol. 120 (2018) 1315–1321.
[40] A.K. Dubey, K. Jeevaratnam, Structural characterization and functional evaluation of an exopolysaccharide produced by *Weissella confusa* AJ53, an isolate from fermented Uttapam batter supplemented with Piper betle L. leaves, Food Sci. Biotechnol. 24 (6) (2015) 2117–2124.
[41] Y. Yang, F. Feng, Q. Zhou, F. Zhao, R. Du, Z. Zhou, Y. Han, Isolation, purification and characterization of exopolysaccharide produced by *Leuconostoc pseudomesenteroides* YF32 from soybean paste, Int. J. Biol. Macromol. 114 (2018) 529–535.
[42] H.-K. Kang, J.-S. Oh, D. Kim, Molecular characterization and expression analysis of the glucansucrase DSRWC from *Weissella cibaria* synthesizing a α (1→6) glucan, FEMS Microbiol. Lett. 292 (1) (2009) 33–41.
[43] M.-S. Kang, J. Chung, S.-M. Kim, K.-H. Yang, J.-S. Oh, Effect of *Weissella cibaria* isolates on the formation of *Streptococcus mutans* biofilm, Caries Res. 40 (5) (2006) 418–425.
[44] J. Jiang, S. Guo, W. Ping, D. Zhao, J. Ge, Optimization production of exopolysaccharide from *Leuconostoc lactis* L2 and its partial characterization, Int. J. Biol. Macromol. 159 (2020) 630–639.
[45] B. Wang, Q. Song, F. Zhao, Y. Han, Z. Zhou, Production optimization, partial characterization and properties of an exopolysaccharide from *Lactobacillus sakei* L3, Int. J. Biol. Macromol. 141 (2019) 21–28.
[46] D. Kavitake, P.B. Devi, S.P. Singh, P.H. Shetty, Characterization of a novel galactan produced by *Weissella confusa* KR780676 from an acidic fermented food, Int. J. Biol. Macromol. 86 (2016) 681–689.
[47] J. Jayamanohar, P.B. Devi, D. Kavitake, S. Rajendran, V.B. Priyadarisini, P. H. Shetty, Characterization of α-D-glucan produced by a probiont *Enterococcus hirae* KX577639 from feces of south Indian *Irula* tribals, Int. J. Biol. Macromol. 118 (2018) 1667–1675.
[48] G. Nikolic, M. Cakic, L. Ilic, Specific refractive index increments of inulin, J. Serbian Chem. Soc. 66 (6) (2001) 397–402.
[49] S. Exarhopoulos, S.N. Raphaelides, M.G. Kontominas, Conformational studies and molecular characterization of the polysaccharide kefiran, Food Hydrocoll. 77 (2018) 347–356.
[50] I. Dueramae, M. Yoneyama, N. Shinyashiki, S. Yagihara, R. Kita, Self-assembly of acetylated dextran with various acetylation degrees in aqueous solutions: studied by light scattering, Carbohydr. Polym. 159 (2017) 171–177.
[51] Y.A. Skorik, V.A. Petrova, O.V. Okatova, I.A. Strelina, E.R. Gasilova, Characterization of clusters and unimers in associating solutions of chitosan by dynamic and static light scattering, Macromol. Chem. Phys. 217 (14) (2016) 1636–1644.
[52] B. Iyisan, K. Landfester, Polymeric nanocarriers, in: P. Gehr, R. Zellner (Eds.), Biological Responses to Nanoscale Particles, Cham, Springer, 2019, pp. 53–84.
[53] T. Bund, S. Allelein, A. Arunkumar, J.A. Lucey, M.R. Etzel, Chromatographic purification and characterization of whey protein–dextran glycation products, J. Chromatogr. A 1244 (2012) 98–105.
[54] R. Hebbar, A. Isloor, A. Ismail, Contact angle measurements, in: N. Hilal, A. F. Ismail, T. Matsuura, D. Oatley-Radcliffe (Eds.), Membrane Characterization, Elsevier, Amnsterdam, 2017, pp. 219–255.